

# Non-linear spherical collapse in tachyon models and a comparison of collapse in tachyon and quintessence models of dark energy

Manvendra Pratap Rajvanshi & J.S. Bagla

Dept. of Physical Sciences, IISER Mohali, Sector 81, SAS Nagar, Punjab (India) - 14036

E-mail: manvendra@iisermohali.ac.in, jasjeet@iisermohali.ac.in

September 2020

**Abstract.** We study evolution of perturbations in dark matter and dark energy for spherical collapse using a completely self consistent, relativistic approach. We study Tachyon models of dark energy using the approach outlined in Rajvanshi and Bagla (2018). We work with models that are allowed by current observations. We find that as with Quintessence models allowed by observations, dark energy perturbations do not affect evolution of perturbations in dark matter in a significant manner. Perturbations in dark energy remain small for such models. We then take two different Lagrangians for dark energy: tachyon and quintessence models, reconstruct potential to have same expansion history and then compare if two can be distinguished in the nonlinear regime. Any variations we find are only due to a different Lagrangian density, and allow a comparison of different classes of models in a fair manner. We find that dark matter perturbations carry no imprint of the class of dark energy models for the same expansion history: this is significant in that we can work with any convenient model to study clustering of dark matter. We find that the evolution of dark energy perturbations carries an imprint of the class of models and dark energy perturbations grow differently in Tachyon models and Quintessence models for the same expansion history. However, the difference between these diminishes for  $(1 + w) \ll 1$  and hence prospects for differentiating between models using characteristics of perturbations are limited in our Universe.

## 1. Introduction

Observations have shown that the Universe is undergoing accelerated expansion [1, 2]. This inference was the result of improvements in determination of cosmological parameters through improved measurement of distances. In particular use of Supernovae type Ia as standardized candles [3, 4, 5, 6] allowed distance determination to be made up to higher redshifts. The observed accelerated expansion spurred developments in theoretical cosmology as the *obvious* explanation, the cosmological constant [7, 8] is riddled with fine tuning and naturalness problems [9, 10, 11, 12]. A number of approaches have been tried: one approach is where Einstein's theory is modified in

some manner [13, 14, 15, 16, 17, 18, 19]. These changes affect the left hand side of Einstein's equation. This approach has to contend with the remarkable success of the general theory of relativity when confronted by observational tests [20, 21, 22]. The other leading approach is the introduction of a constituent that mimics the cosmological constant in an approximate manner. This additional component, the so called dark energy, is required to have some unusual properties [23, 24, 25, 26]. There are a large number of possibilities that have been proposed and explored in this category. This approach modifies the contents of the Universe and hence it affects the right hand side of Einstein's equations. Each category corresponds to a specific action for a component, in most such models the dark energy couples minimally with other constituents of the Universe. Some examples of such models are scalar fields, K-essence, tachyon models, Chaplygin gas, etc. [27, 28, 29, 30, 31], (see [23] for review). In each of these models the dynamics of the Universe approximates the cosmological constant in order to reproduce accelerated expansion. Present observations allow for small deviations from the cosmological constant model. Thus, there are qualitative and quantitative differences in the dynamics, though each model can be tuned to produce the expansion history required by observations within some reasonable constraints.

A fundamental difference between the cosmological constant and other models is that the cosmological constant does not vary with time or location, whereas other dark energy models allow for such variations. In all other models the dark energy component is allowed to vary and respond to variations in the gravitational field. A number of studies have been carried out to study dynamics and perturbations in various dark energy models [32, 33, 34, 35, 36, 37, 28, 40, 41]. The key result of these studies, obtained using linear perturbation theory or other approximations, is that the perturbations in dark energy remain very small. However, perturbation theory is valid only at early times or at very large scales at late times. Thus it cannot be used to study dark energy perturbations and their interplay with highly non-linear dark matter perturbations at small scales.

In an earlier work we have studied fully non-linear evolution of spherically symmetric perturbations in quintessence models of dark energy [42, 43]. We found that the amplitude of dark energy perturbations remains small in all cases. We also found that the effective equation of state parameter of dark energy becomes a function of coordinates and this variation is correlated with the density contrast of dark matter.

Here we use the same methodology and study tachyon models for dark energy. There are low energy effective theories that arise from string theory that contain tachyon fields [38] with Lagrangian:

$$\mathcal{L} = -V(\psi)\sqrt{(1 - \partial^\mu\psi\partial_\mu\psi)} \quad (1)$$

Here  $\psi$  is tachyon field and  $V(\psi)$  is potential. As an analogy, if one sees quintessence a field form of classical particle Lagrangian(kinetic term+ potential part), then tachyon Lagrangian is field form of Lagrangian for relativistic particle. Tachyon models and their characteristics have been studied in detail[37, 28]. As shown in [28], some

potentials (particularly exponential potential  $V \propto e^{-\psi}$ ) have interesting asymptotic future behavior with the possibility to avoid future horizon. There have also been some attempts to unify dark matter and dark energy in terms of a single tachyon field [39]. Here, inverse square potential ( $V \propto \psi^{-2}$ ) as a function of field  $\psi$  averaged over some scale gives a dark matter like behaviour at certain scales. While quintessence models have been extensively studied in context of various types of perturbations, tachyonic models have not been studied in as much detail (see [41] for study of linear perturbations in tachyon models). Different theoretical motivations/insights might lead to different class of models, but there has to be framework that can be used to distinguish different type of models. It is in this context, that we carry on from our previous work[42] where we simulated spherical collapse for quintessence, modify the formalism for tachyonic field and do a systematic comparison. We study two potentials ( $V \propto \psi^{-2}$  and  $V \propto e^{-\psi}$ ) that have been proposed and studied for tachyon models because of their interesting features as discussed above (see [28, 37]). Further, in order to explore the dependence of the growth of perturbations on the class of models, we compare the evolution of perturbations in quintessence models and tachyon models *for the same expansion history*.

We describe the formalism and equations in §2. Details of the expansion history in models to be studied is discussed in §3 for two potentials studied here for tachyon models. Evolution of perturbations for dark matter and dark energy in these cases is described in §4. We then proceed to compare quintessence and tachyon models by working with potentials that give us the same expansion history. These are discussed in §5. Results are summarised in §5.1 and §5.2, dealing with dark matter properties and dark energy properties respectively.

## 2. Equations and Formalism

We follow the scheme set out in Rajvanshi and Bagla [42, 43] and refer the reader to the paper for more details.

We assume spherical symmetry and treat dark matter as a pressure-less fluid. Tachyon models are described by the following Lagrangian density:

$$\mathcal{L} = -V(\psi)\sqrt{(1 - \partial^\mu\psi\partial_\mu\psi)} \quad (2)$$

Space-time is described by the following metric:

$$ds^2 = -e^{(2B)}dr^2 - R^2(d\theta^2 + \sin^2\theta d\phi^2) + dt^2 \quad (3)$$

where  $B(r, t)$  and  $R(r, t)$  are unknown functions of comoving radial coordinate  $r$  and time  $t$ .

These allow us to obtain dynamical equations for all the variables in the system.

Note: We work in units where speed of light  $c$  and gravitational constant  $G$ , both are unity.  $V$  denotes potential as a function of  $\psi$  and  $V_{,\psi}$  represents gradient of this

potential with respect to  $\psi$ . The full set of equations along with Einstein's equations is:

$$\ddot{B} = -e^{-2B} \frac{R'^2}{R^2} + \frac{1}{R^2} + \frac{\dot{R}^2}{R^2} - \dot{B}^2 - 4\pi\rho_{dm} + 4\pi V \left[ \frac{e^{-2B}\psi'^2 - \dot{\psi}^2}{\sqrt{1-u^2}} \right] \quad (4)$$

$$\frac{\ddot{R}}{R} = \frac{4\pi V}{\sqrt{1-u^2}} [1 - u^2 - e^{-2B}\psi'^2] - \frac{1}{2} \frac{\dot{R}^2}{R^2} + \frac{1}{2} \left[ e^{-2B} \frac{R'^2}{R^2} - \frac{1}{R^2} \right] \quad (5)$$

$$\begin{aligned} \ddot{\psi}RV(e^{2B} + \psi'^2) &= 2e^{-2B}VR'\psi'^3 - 2V\dot{R}\dot{\psi}\psi'^2 + 2VR'\psi'(1 - \dot{\psi}^2) - RV_{,\psi}\psi'^2 \\ &\quad - RVB'\psi'(1 - \dot{\psi}^2) + RV\psi''(1 - \dot{\psi}^2) - 2RV\dot{\psi}\dot{B}\psi'^2 \\ &\quad + 2RV\dot{\psi}\psi'\dot{\psi}' - RV_{,\psi}e^{2B}(1 - \dot{\psi}^2) \\ &\quad - V\dot{\psi}(1 - \dot{\psi}^2)(R\dot{B} + 2\dot{R})e^{2B} \end{aligned} \quad (6)$$

$$\rho_{dm} = - \left( \dot{B} + \frac{2\dot{R}}{R} \right) \rho_{dm} \quad (7)$$

where  $u^2 = \partial^\mu \psi \partial_\mu \psi$  and  $\rho_{dm}$  represents dark matter density.

Here a prime represents a partial derivative with respect to  $r$  and a dot represents a partial derivative with respect to  $t$ .

We study evolution of perturbations for two potentials with tachyon models, details of the potentials are given in the following discussion.

In order to compare evolution of perturbations in tachyon models with quintessence models, we work with potentials that lead to the same expansion history. Methods for computing the potential given an expansion history have been developed for a variety of models [44, 45]. This process is often called reconstruction of potentials. We have done these calculations for  $w = \text{constant}$  and Chevallier-Polarski-Linder(abbreviated as "CPL" from here on, see equation 9) parametrization for quintessence and tachyon models, details of the approach are given in [46].

### 2.1. Computational Methods

We consider a 1-d discrete grid in radial variable  $r$ , and the dependent variables (fields and their first time derivatives) are simulated on this grid as a function of  $r$  which are evolved in time using fourth order Runge-Kutta scheme(RK-4). At each time instant  $t_i$  we calculate all spatial derivatives using finite difference schemes, this allows us to write all first order time derivatives(including derivatives of 1st time derivatives i.e. accelerations) of dependent variables as functions of quantities at  $t_i$ . These functions allow us to get prediction for 1st sub-step of RK-4 scheme and temporary values of all dependent variables which are used for calculations of further sub-steps. This process is repeated until the time for the final intended output is reached. We check for numerical stability and convergence by running for different time steps. The computational methodology is described in detail in paper I[42].

### 3. Results: Background Evolution

We use two potentials for tachyon models that have been studied extensively. We study the background evolution for potentials  $V \propto \psi^{-2}$  and  $e^{-\psi}$ . Figure 1 shows the evolution of density parameters for the tachyon field and dark matter, and the equation of state parameter ( $w$ ). Although each of these potentials has a unique asymptotic behaviour[28], here we have tuned the parameters such that they satisfy observational constraints [40]. Both the models shown here have a thawing behaviour. These plots illustrate the generic behaviour in tachyon models that is consistent with observations. More details for background evolution and comparison with observations can be found in the detailed study by Singh et. al [40].

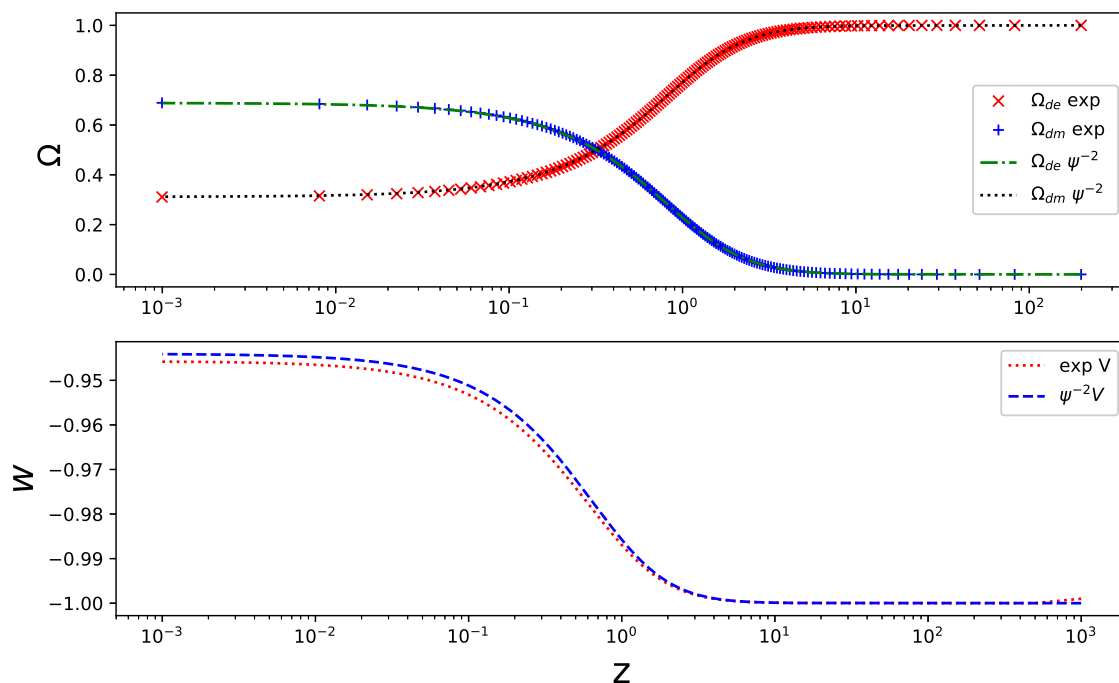


**Figure 1.** Energy densities(Upper Panel) contribution of dark matter and dark energy as a function of redshift( $z$ ). Bottom panel show the evolution of equation of state( $w$ ) of tachyon field. Both backgrounds are very similar in terms of observations with slight difference in effective equation of state parameter( $w$ ).

### 4. Evolution of perturbations

We study perturbations in dark matter and dark energy for two potentials: the exponential potential and the inverse square potential. The initial conditions are set such that the dark matter does not have any peculiar velocities at the initial time. Dark matter has an initial density perturbation. This initial density perturbation has

a compensated profile i.e.  $\delta_{dm}$  integrated from center to outermost radius comes out to be zero, so that average density contrast is 0. Please see [42] for details of initial profile. Dark energy is set to have no perturbations at the initial time. We find that such an initial condition quickly leads to the expected adiabatic mode at early times. We start at  $z_{ini} = 10^3$  and evolve the system towards lower redshifts. We first study the evolution of an over-density. A note for figures: In figures we often use scientific notation for quoting numbers i.e. format  $a \times 10^b$  with exponent part quoted on top of figure, so any no. that is quoted on top left of figure has to be multiplied to y-axis values to get actual values. Exponents are in powers of 10. For example, in figure 3, one has to multiply  $10^{-9}$  to y values. Figure 2 is a plot of dark matter density contrast at the time when the inner regions begin to virialize at  $z \simeq 1.5$ .

The overdensity has been evolved from  $z \sim 1000$ . This is for an initially overdense(OD) system. This is shown for the two potentials we are studying and it can be seen that the dark matter density contrast in these two cases is indistinguishable. This similarity results from an almost identical expansion history.

Corresponding plots for density contrast in dark energy are shown in Figure 3. This is for initially overdense (OD) system. At the start of simulation( $z \sim 1000$ ) there was no perturbation in dark energy field, but metric perturbations induce perturbations in dark energy sector which grow with time. We see that the perturbation in dark energy is very small for the two cases, but there are apparent differences in the two curves.

The dark matter perturbation reaches maximum radius, called the turn around radius, before collapsing back and eventually reaching dynamical or virial equilibrium. The ratio of virial to turn around radius is plotted in Figure 4. It is apparent from this plot that there is no discernable difference in the values for the two potentials mainly because of a similar expansion history.

We now turn our attention to evolution of an under-dense region. While an under-dense region is limited to  $\delta_{dm} \geq -1$ , whereas the density contrast for an over-dense region can be very large. On the other hand, a realistic over-dense region with a large density contrast cannot be arbitrarily large in size, whereas underdense regions can easily be tens of Mpc across. In terms of analysis, we also avoid losing information inside the virialized region as the equations cannot be solved self consistently in this region [42, 43].

The dark energy perturbations are shown in Figure 5. The density contrast is significant over the scale of the under-dense region. We also observe a rapid growth of dark energy perturbations at late times, even though the amplitude of perturbations remains small at all times. We see some variation between the two potentials but it remains at a few percent level and this can be attributed to the difference in expansion history.

We note that the qualitative behaviour of perturbations in dark matter and dark energy closely follows that seen for quintessence models studied earlier [42, 43]. In the following discussion we focus on a comparison of quintessence and tachyon models for the same expansion history.

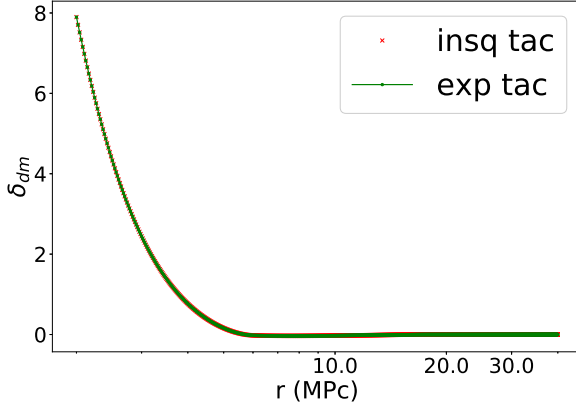


**Figure 2.** Dark matter density contrast as a function of comoving radius at  $z \sim 1.5$ . The two curves correspond to two different dark energy potentials. Label 'insq' refers to  $V \propto \phi^{-2}$  and 'exp' refers to  $V \propto \exp$ .

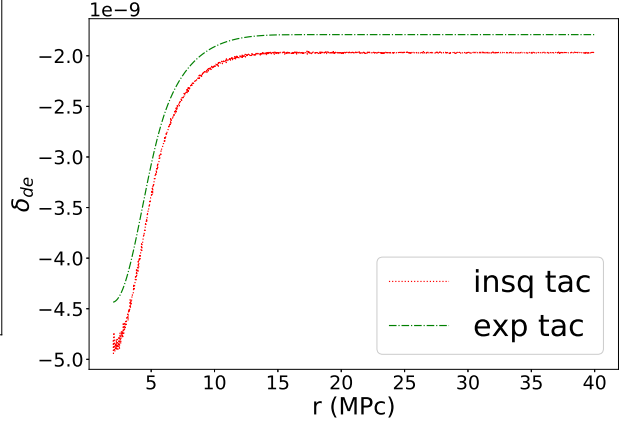


**Figure 3.** Dark energy density contrast as a function of comoving radius at  $z \sim 1.5$ . Label 'insq' refers to  $V \propto \phi^{-2}$  and 'exp' refers to  $V \propto \exp$ .

## 5. Results: Evolution of Perturbations in Quintessence vs Tachyon Models

In order to compare perturbations in tachyon vs quintessence models of dark energy, we reconstruct potentials in both models that correspond to the same expansion history. We codify the expansion history by the variation of the equation of state parameter for dark energy with the scale factor  $w(a)$ . Details of the procedure adopted for computing the potential are given in [46]. We work with two different forms for  $w$  for this comparison:  $w = \text{constant}$  and CPL [44, 45]. We choose three values of constant  $w$  for comparison and numerically reconstruct the corresponding potentials for quintessence and tachyonic fields,

$$w = -0.5, \quad w = -0.9 \quad \text{and} \quad w = -0.975 \quad (8)$$

and for CPL parametrization [44, 45] with form  $w(a)$ :

$$w = w_0 + w_a \left(1 - \frac{a}{a_0}\right) \quad (9)$$

we have  $w_0 = -0.9$  and  $w_a = \pm 0.09$ . That is, the present day equation of state parameter is  $-0.9$  in both the cases but in one case it decreases as we go to earlier epochs, and in the other it increases as we go to earlier epochs. In figures we represent cases with  $w_a = +0.09$  with notation "cpl+" and  $w_a = -0.09$  model with "cpl-". We investigate turn around and virialization characteristics for overdense regions for these cases.

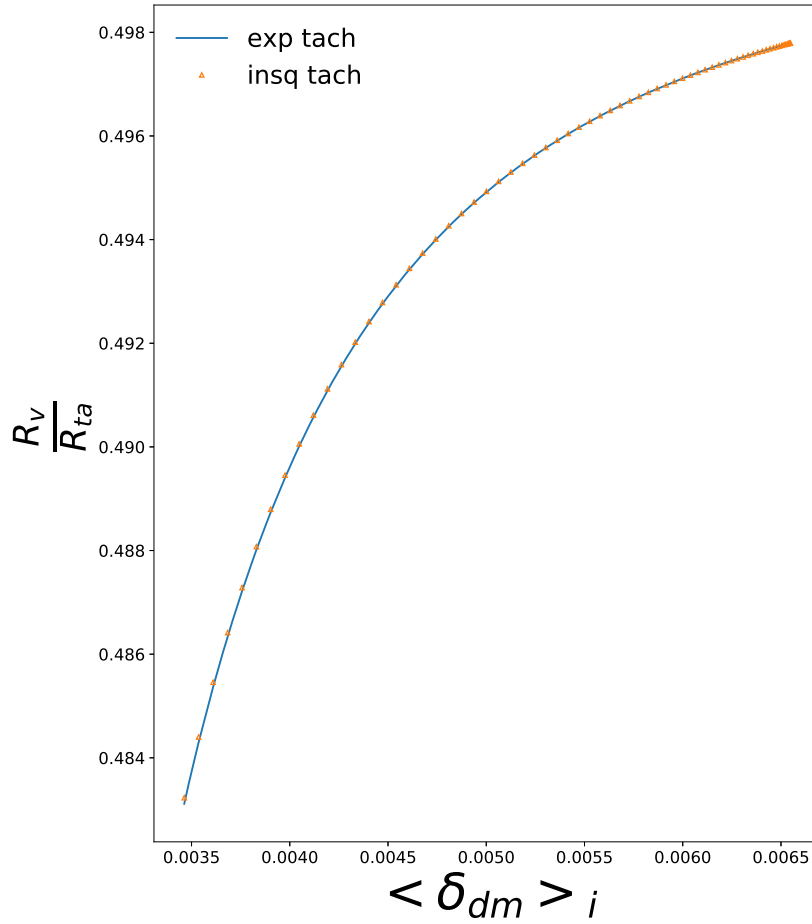


**Figure 4.** Ratio of virial radius to turn around(maximum) radius as a function of initial matter overdensity averaged over interior  $r$  till that particular  $r$ . The ratio tends toward Einstein-DiSitter value of 0.5 as the initial overdensity tends to infinity i.e. dark energy effects on perturbation become less significant as dark matter perturbation become stronger.

### 5.1. Dark Matter Perturbations

We have run our simulations setting initial conditions in the early universe (at  $z \sim 1000$ ) for underdense and overdense dark matter perturbations. We start with an unperturbed dark energy (see [42, 43] for details of initial conditions). The density contrast at present time is shown in figure 6 for constant  $w$  for underdense initial condition. We see that the density contrast for different expansion histories differs from each other but *there is no difference in the profile for quintessence and tachyon models*. This clearly implies that the choice of dark energy model (tachyon or quintessence) has no discernable impact on dark matter density profiles in an underdense region as long as the expansion history is the same. Next we proceed to study the same in the two cases for the CPL parameterization. We refer to models by the sign of the term  $w_a$  and  $w_0$  is same in the two cases ( $w_0 = -0.9$ ). The two cases differ as we have  $w_a = \pm 0.09$ . We show the dark matter density profile for the same initial condition as above in Figure 7. Again, we find



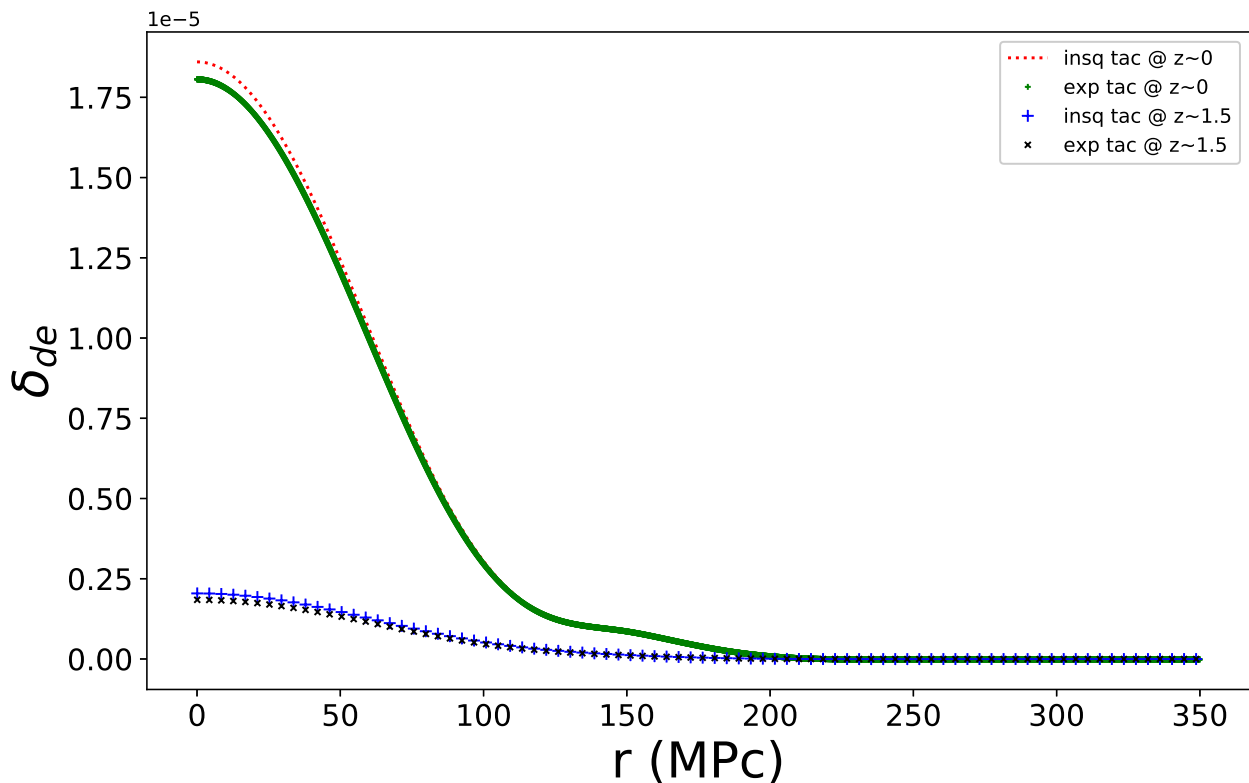


**Figure 5.** Dark energy(DE) density contrast as a function of comoving radius at two different redshifts. Here the initial matter perturbation was underdense. There was no perturbation in DE at initial time, but metric perturbations induce perturbation in DE field. This perturbation grows stronger with time as can be seen from curves at 2 different redshifts.

that there are distinctions between the two cases with a different expansion history but there is no discernable difference in the dark matter density profile for the two different models of dark energy. This is remarkable. Note that bump in contrast around 150 Mpc is because of the compensating overdense region at edge of void to ensure that we go over to an FLRW universe at large  $r$ .

We now turn our attention to growth of overdensities in dark matter. In these cases the perturbations collapse to form virialized halos if the initial density is higher than a critical value as in the case for  $\Lambda$ CDM [47]. Results for the two CPL parameterizations are shown here. We show the characteristics of perturbations at turn around in Figure 8. Variation of the turn around radius as compared to the expected value in the Einstein-deSitter model as a function of the initial overdensity is shown in the left panel. The right panel shows the density contrast at turn around as a function of the initial dark matter overdensity. Note that the overdensities are always volume averaged, so as to facilitate comparison with the Einstein-deSitter and the  $\Lambda$ CDM models. The qualitative behaviour seen in the two panels is very similar to what is known for the  $\Lambda$ CDM model

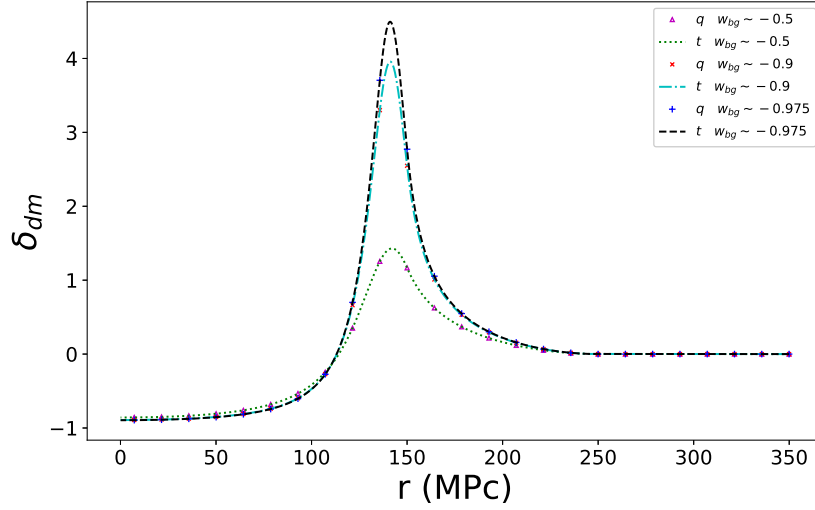


**Figure 6.** Underdense cases constant  $w$  comparison: Dark matter density contrast evolved to  $z \sim 0$ . "q" refers to quintessence models while "t" for tachyonic models. " $w_{bg}$ " is constant value of background  $w$ . Curves are clustered by background histories with quintessence and tachyonic models with same background having indistinguishable matter perturbation dynamics.

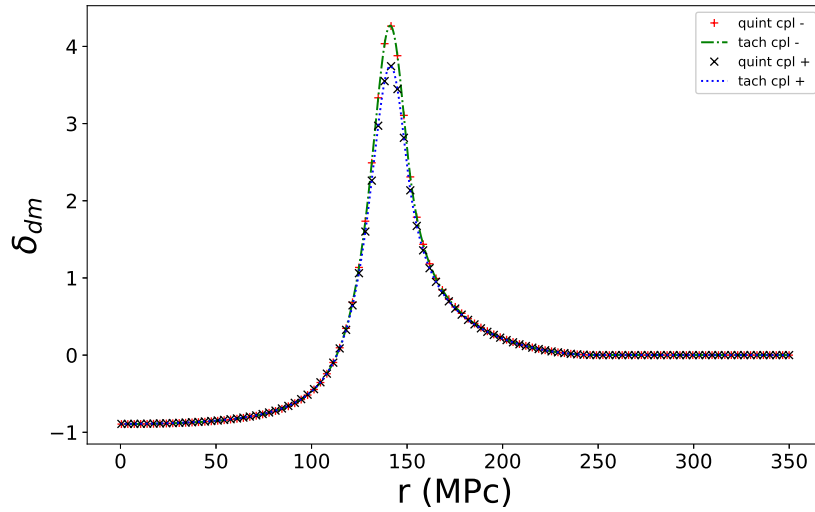


**Figure 7.** Underdense cases CPL: Dark matter density contrast evolved to  $z \sim 0$ . cpl+ denotes  $w_a = +0.09$  case and cpl- represents  $w_a = -0.09$ . "quint" stands for quintessence and "tach" stands for tachyonic. As with constant  $w$  cases, it is background evolution that is distinguishing the models rather than field dynamics Lagrangian being quintessence or tachyonic type.

in that the turn around radius becomes very large as we approach the critical initial overdensity from above. The density contrast also increases in this limit as the time taken to reach turn around increases and the background also increases and the average

density of the universe decreases to give us an enhanced density contrast. The two CPL models representing two different expansion histories lead to different curves. However, there is no obvious difference between the tachyon and quintessence models for a given expansion history.

We present the characteristics of virialization in Figure 9. We have plotted the ratio of the virial radius to the turn around radius in the left panel as a function of the initial density contrast. The expected value for this ratio is 0.5 in the Einstein-deSitter model. In case dark energy clusters significantly and also participates in the virialization process, the expected value is above 0.5, and if dark energy clustering is not relevant to the virialization process then the expected value is below 0.5 [48]. In the right panel we have plotted the density contrast at the time of virialization. Here, virialization is defined by the epoch at which

$$\langle T \rangle + \frac{1}{2} \langle R F_R \rangle = 0 \quad (10)$$

here  $T$  is the kinetic energy,  $R$  is the radius of the shell and  $F_R$  is the radial force on the shell, see [42] for details. Thus the volume averaged overdensity within a virialized shell is expected to be around 145 in Einstein-deSitter model. In the  $\Lambda$ CDM model, the expected value is higher as perturbations take a longer time to collapse. Further, as we approach the critical density contrast for collapse from above, the density contrast at virialization shoots up. Similar behaviour is observed for quintessence models [42, 43]. We see that the qualitative behaviour for the two CPL cases is similar to that for  $\Lambda$ CDM and that seen for some quintessence models. The ratio of virial radius to the turn around radius varies almost in the same manner for the two CPL models with small differences for large initial density contrast. There are no systematic differences between tachyon and quintessence models for a given CPL prescription for the equation of state parameter. Curves for the two CPL models differ clearly from each other in the right panel but again, there are no differences between tachyon and quintessence models for a given set of CPL parameters.

These results are remarkable in that it appears that we can ignore the precise choice of dark energy model and use any convenient prescription as long as we get the same expansion history. This can be done if our interest is restricted to perturbations in dark matter.

## 5.2. Perturbations in Dark Energy

We now turn our attention to perturbations in dark energy. We study two physical quantities, density contrast for dark energy  $\delta_{de}$  and the equation of state parameter  $w$ . These are shown as a function of radius for an initially underdense matter perturbation. We have plotted  $\delta_{de}$  as a function of  $r$  for constant  $w$  cosmologies in Figure 10(upper panel). Curves are plotted at  $z = 0$  and refer to the simulations used in Figure 6. We see that density contrast in dark energy remains small at all scales. The amplitude of dark energy perturbations is higher when the model deviates significantly from  $\Lambda$ CDM: we

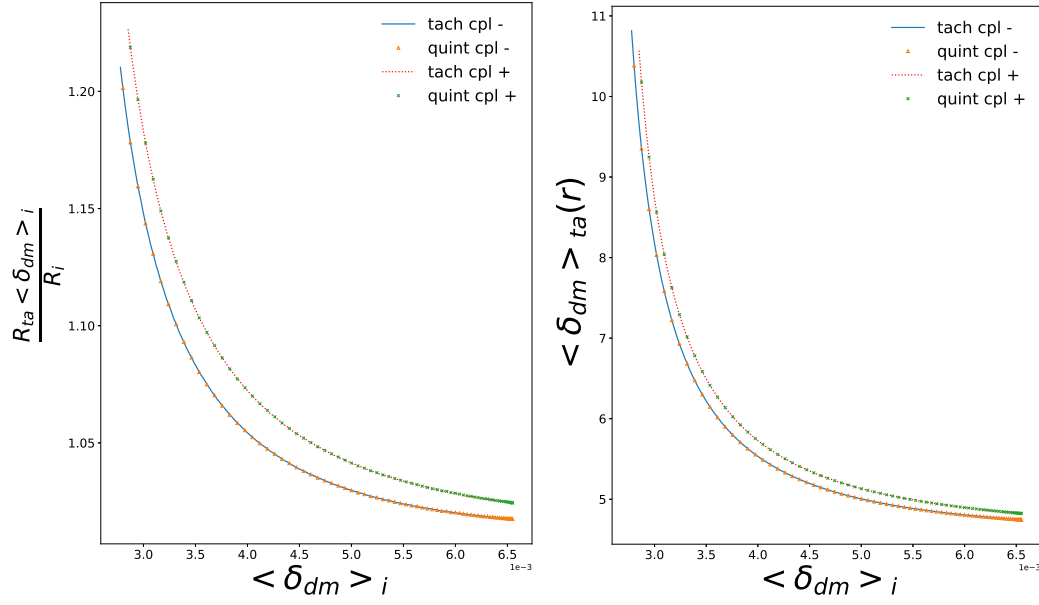


**Figure 8.** Turn around characteristics for CPL case. Left panel shows turn around radius in the combination  $R_{ta} \langle \delta_{dm} \rangle_i / R_i$  as a function of the initial density contrast. Right panel shows density contrast at turn around as a function of the initial density contrast. quint denotes quintessence and tach represents tachyonic field. cpl+ denotes  $w_a = +0.09$  and cpl- represents  $w_a = -0.09$ .

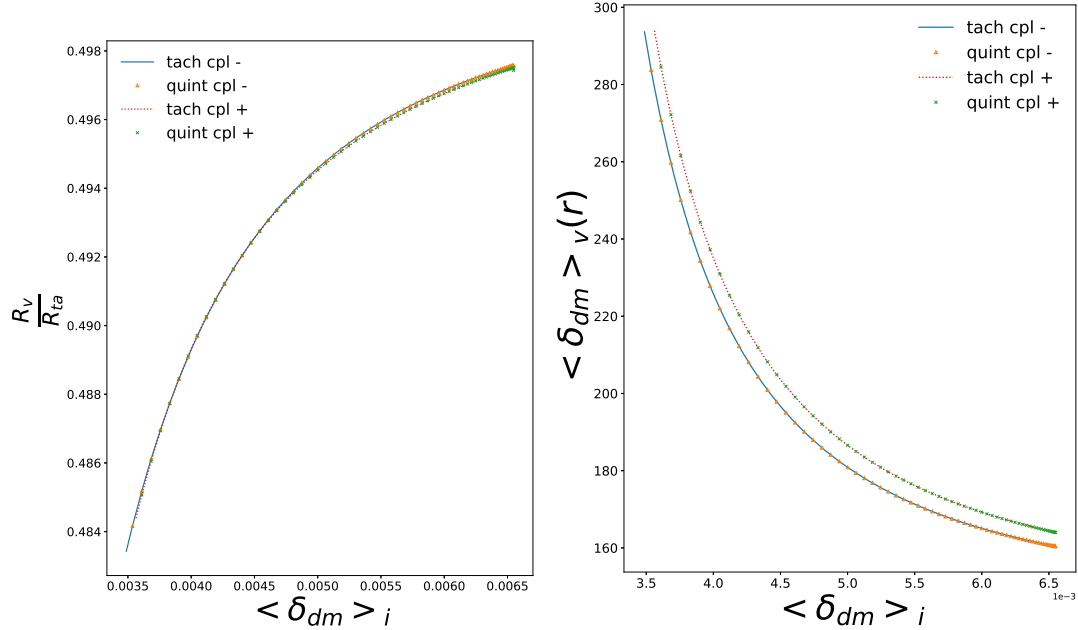


**Figure 9.** Virial characteristics for CPL case. Left panel shows ratio of virial radius to turn around radius as a function of the initial density contrast in dark matter. Right panel shows Density contrast at virialisation as a function of the initial density contrast in dark matter. "quint" denotes quintessence and "tach" represents tachyonic field. cpl+ denotes  $w_a = +0.09$  and cpl- represents  $w_a = -0.09$ .

see that the amplitude is highest for the model with  $w = -0.5$  and decreases for models with a smaller  $w$ . We see that the curves for each  $w$  are distinct. We also note that the tachyon models and quintessence models differ from each other and this difference is larger for models with a larger  $w$ . We have shown in earlier work that  $w$  becomes a function of space for dynamical dark energy models. Variations from the expected value in the background for constant  $w$  models is shown in Figure 10 (lower panel) as a function of  $r$ .

We see that for an underdensity in matter,  $w$  is smaller than the value in the background model. Deviations are larger for models that deviate significantly from the  $\Lambda$ CDM models. Differences between tachyon models and quintessence models can be seen and these are larger for the models with a larger  $w$ .

Plots for CPL models are given in Figure 11. Both the models here are consistent with most low redshift observations [49]. We keep  $w_0 = -0.9$  and  $w_a = \pm 0.09$ , we refer to these models as *cpl+* or *cpl-* depending on the sign of  $w_a$ . These figures refer to the simulations used for Figure 7. Quantities are plotted at  $z = 0$ . We see that there are differences between the tachyon and quintessence models for each CPL model but the differences remain small at all scales.

Unlike dark matter, we find that dark energy perturbations do carry an imprint of the model. Differences between tachyon and quintessence models for the same expansion history become larger for models with large deviations from the  $\Lambda$ CDM model. Differences are small for constant  $w$  models allowed by observations.

## 6. Summary

We have presented results of our study of evolution of perturbations in dark matter and tachyon models of dark energy. We find that differences across models arising from different potentials are small. As different potentials correspond to different expansion history, it is difficult to delineate the dependencies.

In order to study the dependence of evolution of perturbations on the class of models, we construct potentials in quintessence and tachyon models corresponding to constant equation of state  $w$  for dark energy and CPL parameterization. This allows us to address the question of the dependence of evolution of perturbations on the class of models.

We study spherically symmetric perturbations using a self-consistent relativistic code. We study evolution of regions where dark matter is underdense/overdense.

We find that evolution of dark matter perturbations depends only on the expansion history. There is no discernable imprint of the dark energy model on the evolution of dark matter perturbations.

Dark energy perturbations remain small in all cases studied here. The amplitude of dark energy perturbations depends on the expansion history as well as the dark energy model (tachyon/quintessence). *Thus in principle there is an observable signature of the class of dark energy models, though the differences are very small.* These differences

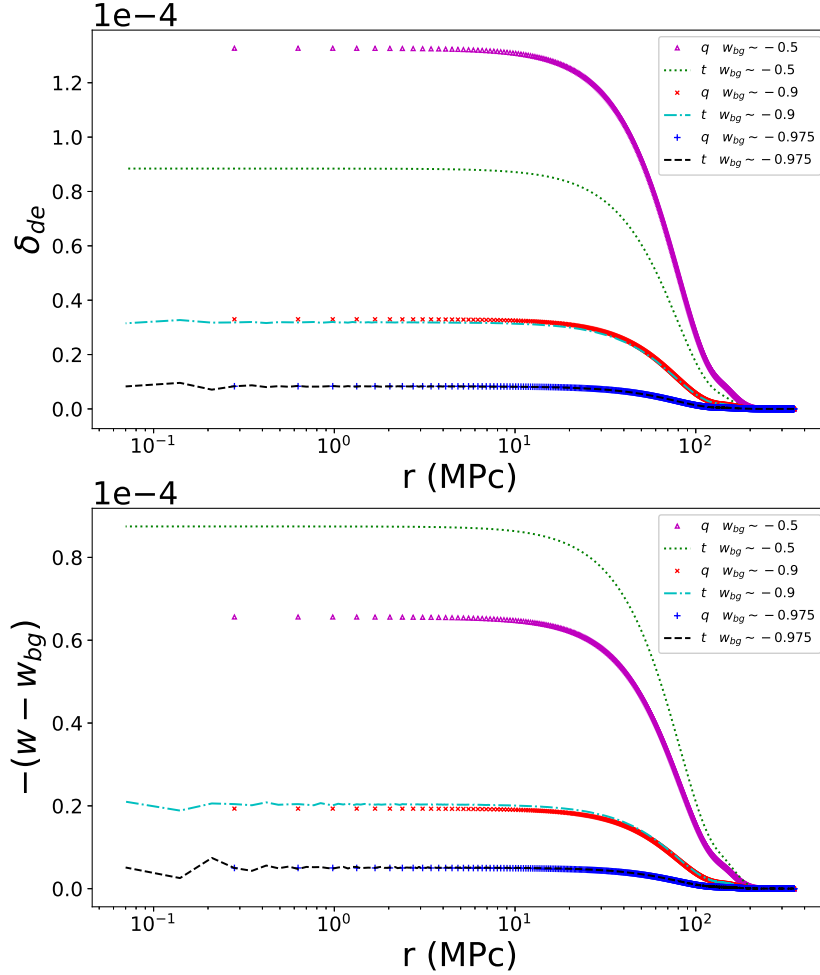


**Figure 10.** Underdense case:(Upper panel) Dark energy density contrast evolved to  $z \sim 0$ .  $q$  denotes quintessence and  $t$  represent tachyonic field.  $w_{bg}$  for constant value of background equation of state for dark energy field. This is for initially underdense case(UD1). Lower panel: Equation of state comparison for three constant equation of state cases.

are larger for models that deviate significantly from the  $\Lambda$ CDM model in terms of the expansion history.

While the results follow from well defined theoretical models and numerical calculations, it is useful to have some physical insight. One can argue from continuity that as one goes towards the  $\Lambda$ CDM limit of  $w = -1$ , all models should converge to  $\Lambda$  like behaviour. One crucial point to check here is for the deviations of  $w$  from  $-1$ , that are allowed by observations, can different models be distinguished by perturbations? In this article we have done nonlinear calculations to probe this question. One of the key takeaways from our work is that the two classes of models considered here

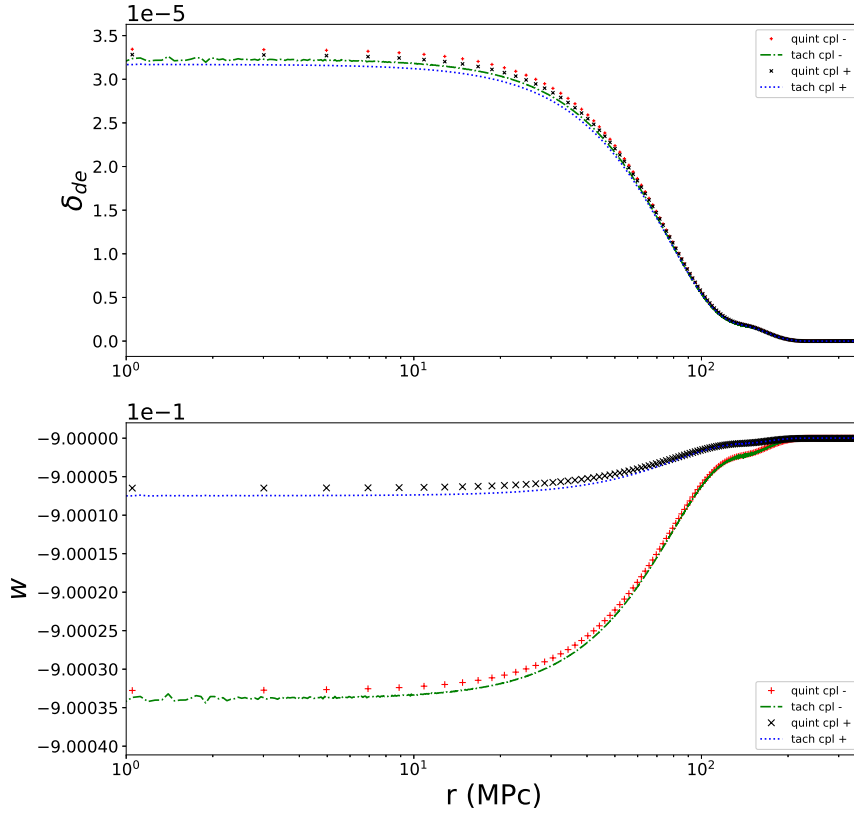


**Figure 11.** Underdense CPL case:(Upper Panel) Dark energy density contrast evolved to  $z \sim 0$ . q denotes quintessence and t represent tachyonic field. cpl+ denotes  $w_a = +0.09$  and cpl- represents  $w_a = -0.09$ . This is for initially underdense case(UD1cpl). Lower Panel: Equation of state( $w$ ) evolved to  $z \sim 0$ . This is for initially underdense case(UD1cpl).

are indistinguishable not only for cases very close to  $\Lambda$  limit, but are so even for scenarios which are significantly different from  $\Lambda$  limit. The above statement applies to characteristics of dark matter perturbations. We believe that this is due to matter being the dominant component for much of the expansion history and matter dominating over dark energy in regions with high overdensity of matter. While this has been pointed out in studies based on linear theory or heuristic arguments, we believe that the calculations presented in this manuscript establish this for the first time with self consistent and relativistic calculations in the non-linear regime.

The useful conclusion that we can draw from this study is that we may choose any dark energy model to reproduce the appropriate expansion history as the evolution of dark matter perturbations is insensitive to the specifics of the dark energy model other than the expansion history.

At the same time, the very small magnitude of differences of dark energy

perturbations indicate that it will be almost impossible for us to discover the true dark energy model from measurements of distances or characteristics of dark matter perturbations.

## Acknowledgments

Authors acknowledge useful discussion with Harvinder K. Jassal and Avinash Singh. Computational work was carried out at computing facilities at IISER Mohali. This research has made use of NASA's Astrophysics Data System Bibliographic Services.

## References

- [1] A. G. Riess, A. V. Filippenko, P. Challis, A. Clocchiatti, A. Diercks, P. M. Garnavich, R. L. Gilliland, C. J. Hogan, S. Jha, R. P. Kirshner, B. Leibundgut, M. M. Phillips, D. Reiss, B. P. Schmidt, R. A. Schommer, R. C. Smith, J. Spyromilio, C. Stubbs, N. B. Suntzeff, and J. Tonry, "Observational evidence from supernovae for an accelerating universe and a cosmological constant," *The Astronomical Journal*, vol. 116, pp. 1009–1038, sep 1998.
- [2] S. Perlmutter *et al.*, "Measurements of Omega and Lambda from 42 high redshift supernovae," *Astrophys. J.*, vol. 517, pp. 565–586, 1999.
- [3] M. M. Phillips, "The absolute magnitudes of Type IA supernovae," *apjl*, vol. 413, pp. L105–L108, Aug. 1993.
- [4] M. Hamuy, M. M. Phillips, N. B. Suntzeff, R. A. Schommer, J. Maza, and R. Aviles, "The Absolute Luminosities of the Calan/Tololo Type IA Supernovae," *aj*, vol. 112, p. 2391, Dec. 1996.
- [5] A. G. Riess, W. H. Press, and R. P. Kirshner, "A precise distance indicator: Type ia supernova multicolor light-curve shapes," *The Astrophysical Journal*, vol. 473, pp. 88–109, dec 1996.
- [6] A. G. Riess, W. H. Press, and R. P. Kirshner, "Using Type IA supernova light curve shapes to measure the Hubble constant," *apjl*, vol. 438, pp. L17–L20, Jan. 1995.
- [7] J. P. Ostriker and P. J. Steinhardt, "The observational case for a low-density Universe with a non-zero cosmological constant," *nat*, vol. 377, pp. 600–602, Oct. 1995.
- [8] J. S. Bagla, T. Padmanabhan, and J. V. Narlikar, "Crisis in Cosmology: Observational Constraints on  $\omega$  and  $H_0$ ," *Comments on Astrophysics*, vol. 18, p. 275, Jan 1996.
- [9] S. Weinberg, "The cosmological constant problem," *Rev. Mod. Phys.*, vol. 61, pp. 1–23, Jan 1989.
- [10] P. Bull *et al.*, "Beyond  $\Lambda$ CDM: Problems, solutions, and the road ahead," *Phys. Dark Univ.*, vol. 12, pp. 56–99, 2016.
- [11] J. F. Navarro and M. Steinmetz, "The core density of dark matter halos: a critical challenge to the lambda-cdm paradigm?," *Astrophys. J.*, vol. 528, pp. 607–611, 2000.
- [12] A. Del Popolo and M. Le Delliou, "Small scale problems of the  $\Lambda$ CDM model: a short review," *Galaxies*, vol. 5, no. 1, p. 17, 2017.
- [13] T. Clifton, P. G. Ferreira, A. Padilla, and C. Skordis, "Modified Gravity and Cosmology," *Phys. Rept.*, vol. 513, pp. 1–189, 2012.
- [14] B. Boisseau, G. Esposito-Farèse, D. Polarski, and A. A. Starobinsky, "Reconstruction of a scalar-tensor theory of gravity in an accelerating universe," *Phys. Rev. Lett.*, vol. 85, pp. 2236–2239, Sep 2000.
- [15] Y. Fujii and K. ichi Maeda, "The scalar-tensor theory of gravitation," *Classical and Quantum Gravity*, vol. 20, pp. 4503–4503, sep 2003.
- [16] T. P. Sotiriou and V. Faraoni, "f(R) Theories Of Gravity," *Rev. Mod. Phys.*, vol. 82, pp. 451–497, 2010.
- [17] A. A. Starobinsky, "Disappearing cosmological constant in f(R) gravity," *JETP Lett.*, vol. 86, pp. 157–163, 2007.



- [18] S. Nojiri and S. D. Odintsov, Phys. Rept. **505**, 59-144 (2011) doi:10.1016/j.physrep.2011.04.001 [arXiv:1011.0544 [gr-qc]].
- [19] S. Nojiri, S. Odintsov and V. Oikonomou, Phys. Rept. **692**, 1-104 (2017) doi:10.1016/j.physrep.2017.06.001 [arXiv:1705.11098 [gr-qc]].
- [20] C. M. Will, “The Confrontation between General Relativity and Experiment,” *Living Rev. Rel.*, vol. 17, p. 4, 2014.
- [21] N. Yunes and X. Siemens, “Gravitational-wave tests of general relativity with ground-based detectors and pulsar-timing arrays,” *Living Reviews in Relativity*, vol. 16, p. 9, Nov 2013.
- [22] B. Jain and P. Zhang, “Observational tests of modified gravity,” *Phys. Rev. D*, vol. 78, p. 063503, Sep 2008.
- [23] L. Amendola and S. Tsujikawa, *Dark Energy*. Jan. 2015.
- [24] T. Buchert, “Dark Energy from Structure: A Status Report,” *Gen. Rel. Grav.*, vol. 40, pp. 467–527, 2008.
- [25] D. Huterer and D. L. Shafer, “Dark energy two decades after: Observables, probes, consistency tests,” *Rept. Prog. Phys.*, vol. 81, no. 1, p. 016901, 2018.
- [26] E. J. Copeland, M. Sami, and S. Tsujikawa, “Dynamics of dark energy,” *Int. J. Mod. Phys.*, vol. D15, pp. 1753–1936, 2006.
- [27] B. Ratra and P. J. E. Peebles, “Cosmological Consequences of a Rolling Homogeneous Scalar Field,” *Phys. Rev.*, vol. D37, p. 3406, 1988.
- [28] J. S. Bagla, H. K. Jassal, and T. Padmanabhan, “Cosmology with tachyon field as dark energy,” *Phys. Rev. D*, vol. 67, p. 063504, Mar 2003.
- [29] C. Armendariz-Picon, V. F. Mukhanov, and P. J. Steinhardt, “A Dynamical solution to the problem of a small cosmological constant and late time cosmic acceleration,” *Phys. Rev. Lett.*, vol. 85, pp. 4438–4441, 2000.
- [30] C. Armendariz-Picon, V. F. Mukhanov, and P. J. Steinhardt, “Essentials of k essence,” *Phys. Rev.*, vol. D63, p. 103510, 2001.
- [31] A. Kamenshchik, U. Moschella, and V. Pasquier, “An alternative to quintessence,” *Physics Letters B*, vol. 511, pp. 265–268, Jul 2001.
- [32] M. Doran, C. M. Muller, G. Schafer, and C. Wetterich, “Gauge-invariant initial conditions and early time perturbations in quintessence universes,” *Phys. Rev.*, vol. D68, p. 063505, 2003.
- [33] M. Malquarti and A. R. Liddle, “Evolution of large scale perturbations in quintessence models,” *Phys. Rev.*, vol. D66, p. 123506, 2002.
- [34] L. R. W. Abramo and F. Finelli, “Attractors and isocurvature perturbations in quintessence models,” *Phys. Rev.*, vol. D64, p. 083513, 2001.
- [35] S. Unnikrishnan, H. K. Jassal, and T. R. Seshadri, “Scalar Field Dark Energy Perturbations and their Scale Dependence,” *Phys. Rev.*, vol. D78, p. 123504, 2008.
- [36] H. K. Jassal, “A comparison of perturbations in fluid and scalar field models of dark energy,” *Phys. Rev.*, vol. D79, p. 127301, 2009.
- [37] T. Padmanabhan, “Accelerated expansion of the universe driven by tachyonic matter,” *Phys. Rev. D*, vol. 66, p. 021301, Jun 2002.
- [38] A. Sen, JHEP **07** (2002), 065 doi:10.1088/1126-6708/2002/07/065 [arXiv:hep-th/0203265 [hep-th]].
- [39] T. Padmanabhan and T. R. Choudhury, Phys. Rev. D **66** (2002), 081301 doi:10.1103/PhysRevD.66.081301 [arXiv:hep-th/0205055 [hep-th]].
- [40] Avinash Singh, Archana Sangwan and H. K. Jassal, “Low redshift observational constraints on tachyon models of dark energy,” *jcap*, vol. 2019, p. 047, April 2019.
- [41] A. Singh, H. K. Jassal, and M. Sharma, “Perturbations in Tachyon Dark Energy and their Effect on Matter Clustering,” 2019.
- [42] M. Pratap Rajvanshi and J. S. Bagla, “Nonlinear spherical perturbations in quintessence models of dark energy,” *jcap*, vol. 6, p. 018, June 2018.
- [43] Manvendra Pratap Rajvanshi and J.S Bagla. Erratum: Nonlinear spherical perturbations in quintessence models of dark energy. *Journal of Cosmology and Astroparticle Physics*,

- 2020(03):E01–E01, mar 2020.
- [44] M. Chevallier and D. Polarski, “Accelerating universes with scaling dark matter,” *Int. J. Mod. Phys.*, vol. D10, pp. 213–224, 2001.
  - [45] E. V. Linder, “Exploring the expansion history of the universe,” *Phys. Rev. Lett.*, vol. 90, p. 091301, 2003.
  - [46] M. P. Rajvanshi and J. S. Bagla, *J. Astrophys. Astron.* **40** (2019) no.6, 44 doi:10.1007/s12036-019-9613-2 [arXiv:1905.01103 [astro-ph.CO]].
  - [47] J. D. Barrow and P. Saich, “Growth of large-scale structure with a cosmological constant,” *mnras*, vol. 262, pp. 717–725, Jun 1993.
  - [48] I. Maor and O. Lahav, “On virialization with dark energy,” *JCAP*, vol. 0507, p. 003, 2005.
  - [49] A. Tripathi, A. Sangwan, and H. K. Jassal, “Dark energy equation of state parameter and its evolution at low redshift,” *JCAP*, vol. 1706, no. 06, p. 012, 2017.